Zadvarzi and Amooey
Environmental Sciences Europe (2023) 35:60
https://doi.org/10.1186/s12302-023-00774-9

Environmental Sciences Europe

RESEARCH

Open Access

Amoxicillin and cefixime simultaneous adsorption by facile synthesized chitosan@polyacrylamide@ZIF-8: isotherm and kinetic study

Saber Babaee Zadvarzi[1] and Ali Akbar Amooey[1*]

Abstract

In recent years, taking medicine has been increasing around the world due to population growth and the spread of disease. Antibiotics as a kind of these medicines include about 10 to 15% of drug consumption. Studies show that antibiotics, which are not completely removed, have a permanent and destructive effect on the environment. In this study, the chitosan@polyacrylamide@ZIF-8 as an adsorbent was simultaneously used to remove cefixime and amoxicillin from the aqueous solution by adsorption methods. XRD and FTIR patterns were analyzed to investigate the surface crystallinity and the chemical properties of the adsorbent. In the following, SEM and TEM images were used for surface morphology study. Finally, a numerical investigation was done for predicting the adsorption effective parameters. The results show that pH 4, contact time 30 min, initial concentration 50 mg/L, temperature 25 °C and 15 mg of adsorbent in 10 mL of polluted water are optimal conditions at which a removal percentage of up to 90% was achieved. The Langmuir, Freundlich, Temkin, and Dubinin–Radushkevich isotherms were examined by experimental data and Langmuir model presented the best consistency with the experimental results and the maximum calculated adsorption capacity for amoxicillin and cefixime are 910 mg/g and 588 mg/g, respectively. Pseudo-first order, pseudo-second order and intraparticle diffusion were investigated for kinetic studies. The results of the calculations illustrated the pseudo-second order model has been dominant. Overall, this study expresses, chitosan@polyacrylamide coated by ZIF-8 can be used an appropriate, effective, and economical adsorbent for the adsorption of amoxicillin and cefixime.

Keywords ZIF-8, Amoxicillin, Cefixime, Adsorption

*Correspondence:
Ali Akbar Amooey
aliakbar_amooey@yahoo.com; aamooey@umz.ac.ir
Full list of author information is available at the end of the article

Graphical Abstract

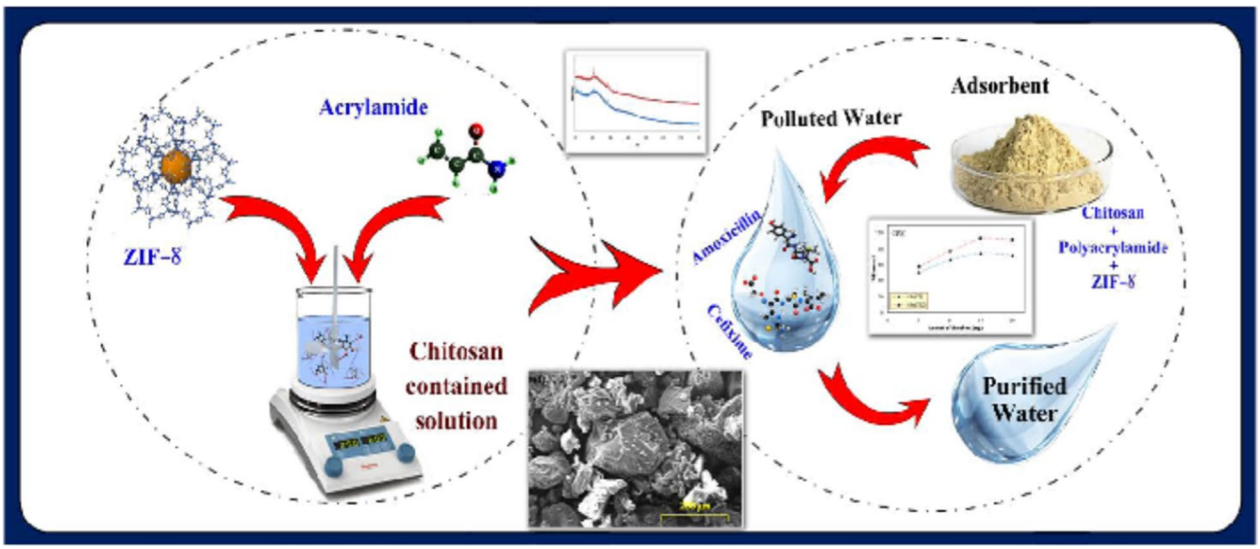

Introduction

Nowadays, water pollution has become a global concern. This causes access limitation to usable water. Therefore, scientists and researchers are seeking appropriate and efficient solutions for water treatment. Some sources that cause water pollution are drugs, even in low concentrations [1]. Among them, antibiotics play an extensive role in various medicines which have a widely endangered influence on public health [2]. The studies show antibiotics have a permanent and destructive effect on the environment which is not completely removed in refineries. [3]. Aquatic environments are influenced by different sources including direct discharge from municipal wastewater remedy plants, human waste, direct disposal of medical, veterinary and industrial squander. In order to eliminate the destructive effects of active bacteria in the treatment, it is necessary to remove the drugs before they enter the wastewater treatment plant [4]. Antibiotics are classified according to their structures; one of the important categories is the antibiotics with a beta-lactam ring in their structure. Accordingly, antibiotics are divided into beta-lactam and non-beta-lactam rings; 32.6% of them belong to the beta-lactam group (penicillin, amoxicillin, ampicillin and cefixime) [5, 6]. Amoxicillin (AMX) is one of the most important groups of antibacterial drugs, which is prescribed for the infections treatment of the body and as an antiviral drug for humans. Even very low concentrations of AMX can pollute the water sources. The molecular structure of AMX is shown in Fig. 1 [7].

Cefixime (CFX) is one of the most important antibiotics used to treat infections and also effectively used against various bacterial organisms and infections, including staphylococcus, hemophilia, *Escherichia coli*, streptococcal fever, tonsillitis and throat infections [8]. The CFX molecular structure is shown in Fig. 2 [9].

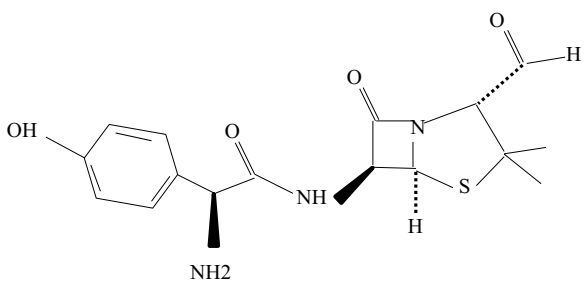

Fig. 1 Molecular structure of AMX

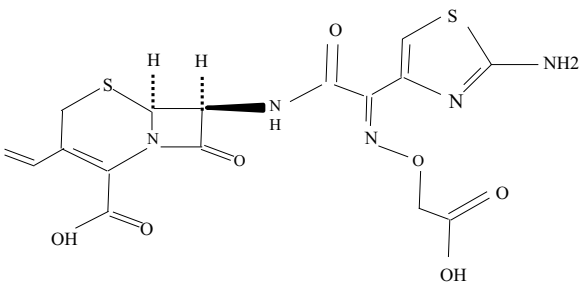

Fig. 2 Molecular structure of CFX

Numerous methods including, reverse osmosis [10], flocculation and coagulation [11], chemical oxidation [12], optical decomposition [13], biological treatment and adsorption have been developed for the treatment of wastewater containing antibiotics [14, 15]. Adsorption process due to low operating costs, high flexibility, insensitivity to toxic compounds and contaminants, lack of secondary material production in the system, high recovery, low consumption of adsorbent, high efficiency and specific surface area for removal, is a promising process to reduce pharmaceutical, heavy metal and dyes [16, 17]. Pham and et al. [18] investigated the adsorption of beta-lactam CFX onto strong polycation, polydiallyldimethylammonium chloride modified nanosilica, and also the adsorption of AMX was examined with MnO_2 nanosheets were in situ grown on biomass carbon microspheres. Also, Adriano and et al. investigated the adsorption of AMX on chitosan beads how have been determined in batch studies. [19]. Adsorption of CFX and lamotrigine on HKUST-1/ZIF-8 nanocomposite was investigated by Emami et al. [20].

These works indicated that using appropriate adsorbent is critical in removal processes, so synthesizing the new adsorbent to simultaneous removal of multi adsorbent is the key term. Metal–organic frameworks (MOFs) have become interesting and important adsorbent for the adsorption of medicines, heavy metals and dyes, mainly due to their high porosity surface area. The framework structure of ZIF-8 is intercalated into zinc metal and 2-methylimidazole ligands. ZIF-8 remarkably increases the adsorption efficiency due to its multifaceted and unique structure [21]. ZIF-8s are collected from tetrahedrally coordinated mutated metal ions such as: Co, Fe, Zn and Cu, coupled by imidazolate linkers [22]. Because AMX and CFX are widely used in the treatment of many diseases, the presence of these drugs in the solution is very destructive, so their removal from the solution before entering the environment is essential [23].

In this study, by adding ZIF-8 to the composite structure of chitosan@polyacrylamide, chitosan@polyacrylamide@ ZIF-8 (CPZ) was synthesized and used as a novel adsorbent to adsorption of AMX and CFX. As strong point, CPZ was used successfully for removing this antibiotics, simultaneously. Herein, we developed a facile and cost-effective strategy to synthesize a composite adsorbent (CP) modified by ZIF-8 (CPZ) that showed excellent adsorption properties. In addition, in examining the influence of effective parameters in the adsorption process, the performance of the CPZ composite was also superior to the CP. Physical properties of CP and CPZ, explored by XRD, FTIR, TEM and SEM. in order to specify optimum parameters, influence different factors such as: the quantity of adsorbent, initial concentration, temperature, contact time and pH in the adsorption process. Isotherm and kinetic models were investigated to determine the predominant equilibrium data and rate of process throughout the adsorption, respectively.

Materials and methods

Materials

Chitosan (medium molecular weight, 96%), acetic acid and amoxicillin provided by Sigma Aldrich, Switzerland. Acrylamide, ammonium persulfate, 99%, *N*,*N*,*N*,*N*-tetramethylethylenediamine (TEMED), methylenebisacrylamide, zinc nitrate, 99% and 2-methylimidazolate were purchased from Merck, Germany, and CFX become acquired from Acros. Other chemicals and analytic grade reagents were commercially available and used in their pure form. The stock solutions were prepared fresh for each experiment.

Preparation of polyacrylamide–chitosan (CS-PAA)

In order to prepare the chitosan/polyacrylamide adsorbent, the first 5 g of chitosan was added to 60 mL of distilled water and stirred for 15 min to obtain a homogeneous suspension. 10 g of acrylamide monomer was added to the suspension, 30 mL solution agitated for 5 min. 1 g of methylene bisacrylamide and 250 mg of ammonium persulfate were dissolved in 30 mL of distilled water, and added to suspension. Finally, 300 µL of tetramethylethylenediamine (TEMED) was added and polymerized at 25 °C. After the polymerization process is completed, the polyacrylamide–chitosan gel is washed with refined water until the outlet water reaches pH 7 and dried at room temperature. The synthesized adsorbent was analyzed in order to characterize the morphology of the composite, and then it was prepared to carry out the adsorption process.

Synthesis of chitosan@polyacrylamide@ZIF-8 (CS-PAA-ZIF-8)

1 g chitosan was added to 20 mL of 1% (v/v) acetic acid solution and blended for 1 h. 2 g of acrylamide was dissolved completely in 10 mL of deionized water, then added to the solution and mixed for 1 h. 400 mg of methylbisacrylamide and 80 mg of ammonium sulfate were dissolved in 10 mL of distilled water, then added to the original solution and stirred for 2 h. 0.86 g of zinc nitrate was dissolved in deionized water and it was added to the solution and mix for 1 h, and then dispersed for 20 min in the ultrasonic bath. 0.96 g of 2-methylimidazole was added into 10 mL of distilled water and after dissolving, was added to the suspension and mixed for 1 h and then dispersed for 15 min in the ultrasonic bath. After raising it with deionized water, the adsorbent (CPZ) was dried at 50 °C and prepared for the next steps of experiments. The

main adsorbent (CPZ) was synthesized and then it was prepared for the adsorption process.

Characterization

In order to determine the surface morphology, scanning electron microscopy (SEM, SNE-4500M, accelerating voltage of 10–20 kv, SEC, South Korea) was utilized. The X-ray diffract meter (XRD, X'Pert Pro, Germany) was done in the range of $2\theta = 0°–80°$ and operating conditions were 40 kV, $\lambda = 1.54$ oA, 30 Ma and 25 oC and used CuKa reflection as a radioactive resource. To identify the CP and CPZ functional groups, Fourier Transform Infrared spectrometry (FTIR, Spectrum 100, PerkinElmer CO.) analysis was done within the run of 500–4000 cm^{-1} utilizing KBr strategy.

Batch experiments procedure

Co-adsorption method was used to adsorption of AMX and CFX from aqueous media. Influential parameters to achieve optimal conditions have been investigated for pH in range between 2 and 8, the amount of adsorbent range between 5 to 25 mg, initial concentration range between 25 and 200 mg/L, contact time 5 and 40 min and temperature between 25 and 65 °C. In similar and previous studies appropriate dosage was approximately as mentioned range, also many tests were carried out to obtain virtual ranges. All experiments were carried out with 10 mL of AMX and CFX solutions, and then adsorbents were added to the prepared solutions and centrifuged at 5000 rpm for 20 min. Finally, the obtained adsorption capacity calculated by following equation [24]:

$$\mathrm{qe} = (\mathrm{Ci} - \mathrm{Ce}) \times V/M, \tag{1}$$

where q_e (mg/g) is the capacity of adsorbent to adsorption of CFX and AMX at equilibrium, Ci and Ce (mg/L) are adsorbate concentrations at equilibrium and initial time, respectively. V(L) is volume of concentration and M(g) is mass of adsorbent.

Removal efficiency was determined as follows [25]:

$$\text{Removal efficiency}(\%) = (\mathrm{Ci} - \mathrm{Ct}) \times 100/\mathrm{Ci}, \tag{2}$$

where Ci is initial equilibrium concentrations and Ct is the equilibrium concentrations of adsorbate.

Results and discussion

Characterization study

Figure 3 shows the XRD pattern of CP and CPZ composite. The peak formed in position $2\Theta = 20$ indicates the presence of Chitosan in the initial composition. Also, the peaks in positions 28 and 35 demonstrate polyacrylamide in this composite. The XRD pattern of the modified adsorbent containing ZIF-8 is shown in Fig. 3. It can be realized by comparing the XRD pattern of CPZ and CP that, in addition to illustrated peaks in CP composite, the peaks have also are present in positions 10 and 13 of CPZ pattern. Obviously by adding a substance to the initial structure an amorphous structure is organized. The peak in the range of 17 to 25 is more broad in Fig. 3, Finally, according to XRD pattern, the present of ZIF-8 in CPZ adsorbent is confirmed [26, 27].

The FTIR spectrum of the CP and CPZ is indicated in Fig. 4. As shown in Fig. 4a, the presence of a peak in 1068 cm^{-1} of the C–O group tensile vibration in chitosan is shown. As shown in Fig. 4a, a peak in cm^{-1}1068 indicates the presence of the tensile vibration of the C–O group related to chitosan. The adsorption band at 12,925 cm^{-1} illustrates C–H aliphatic

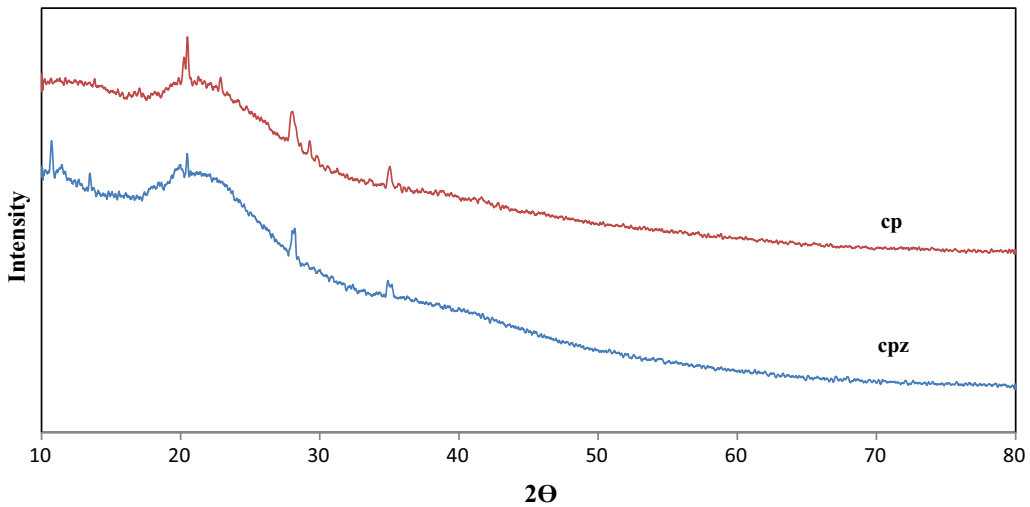

Fig. 3 XRD pattern of CP and CPZ

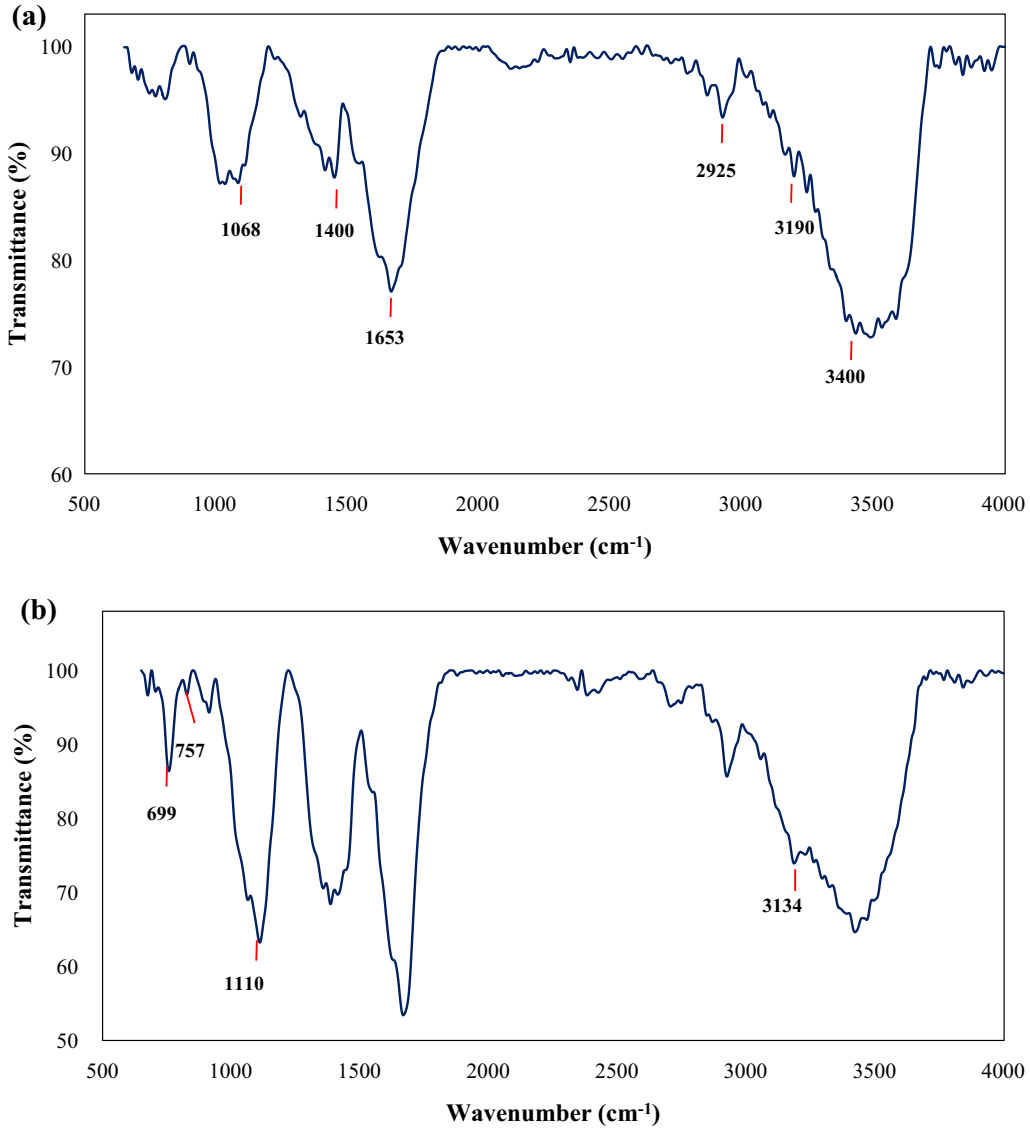

Fig. 4 FTIR spectra of Ch-PAA (**a**) and Ch-PAA-ZIF-8 (**b**)

tensile group in acrylamide and a band at 3400 cm^{-1} corresponds the N–H and O–H groups in chitosan and the amide group in acrylamide. Peak appearance at 1700–1600 cm^{-1} illustrates the overlap of symmetric stretching C=O of chitosan and acrylamide and also adsorption band at 3190 cm^{-1} indicates NH_2 bonding in acrylamide [28]. Asymmetric stretching band of CH_3 related to chitosan appeared at1400 cm^{-1}. According to Fig. 4b, the peaks in 757 cm^{-1} and 699 cm^{-1} show Zn–O and Zn–N bonds, respectively, which confirm that ZIF-8 was loaded in the CPZ structure. The peak at 3134 cm^{-1} corresponding to C–H bond of aromatic and aliphatic tensile of imidazole ring and also, the peak at 1110 cm^{-1} regarding to the tensile vibration of ZIF-8, has not been seen in the CS-PAA spectrum, so it confirms the presence of ZIF-8 in the composite clearly [29, 30].

Figure 5 shows the SEM image of the CP (a, b) and CPZ (c, d). Both of synthesized adsorbents have rough and non-smooth surface. CPZ has a rougher surface than CP which increases the specific surface area of the CPZ adsorbent compared to CP. Furthermore, porosity can also be seen in CPZ surface which has improved the adsorbent properties. Another factor that observable in the SEM review is the proper distribution of ZIF-8 in the absorbent structure and there is not phase separation among the ZIF-8 and composite. Finally, the existence of ZIF-8 in CPZ structure led to adsorption

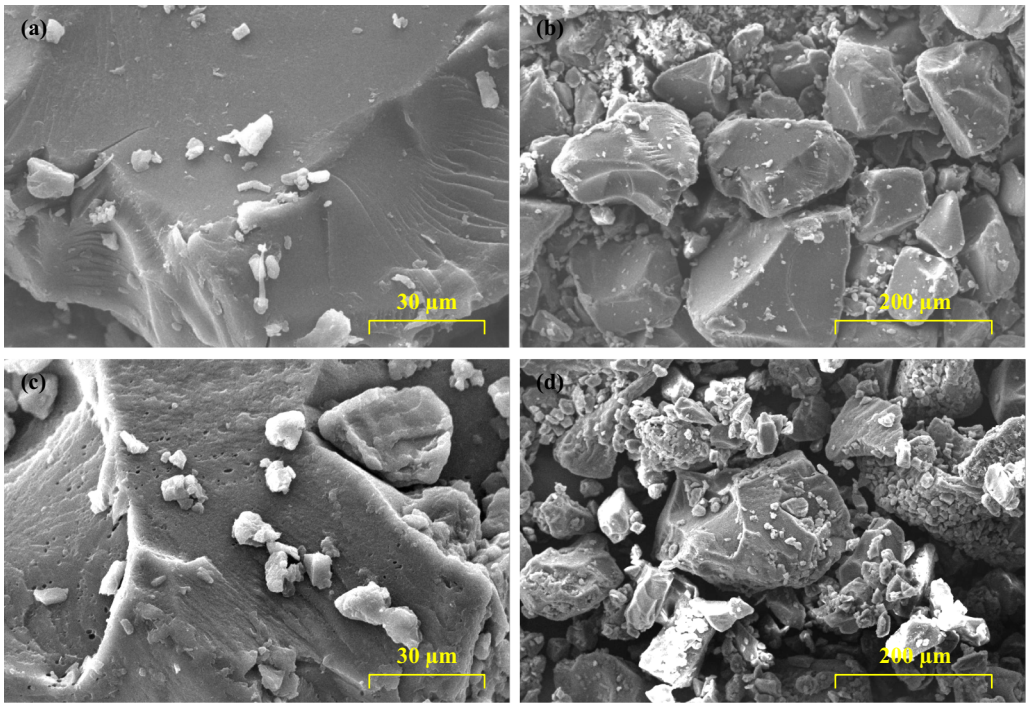

Fig. 5 SEM image of CP (**a**, **b**) and CPZ (**c**, **d**)

performance enhancement by effective parameters such as specific surface area and porosity of the final composite [31].

TEM images related to CP and CPZ are shown in Fig. 6. In Fig. 6a, the physical accumulation of chitosan and polyacrylamide nanoparticles, suitable dispersion and distribution of particles related to chitosan@polyacrylamide is obvious. Dark spots and regular particle size in Fig. 6b indicate the presence of ZIF-8 in the chitosan–polyacrylamide polymer matrix. The regular distribution

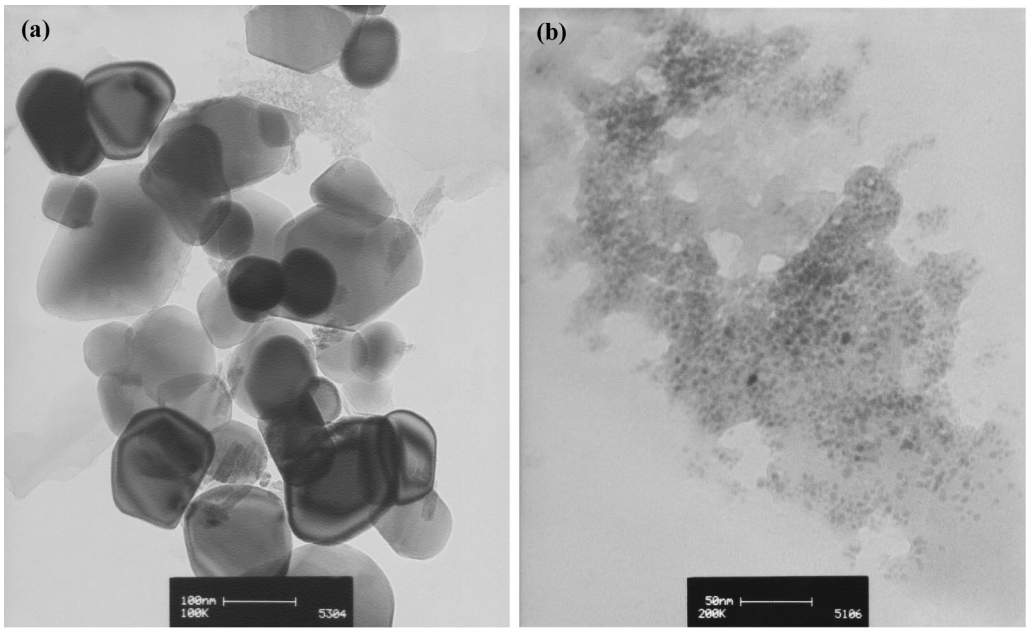

Fig. 6 TEM image of CP (**a**) and CPZ (**b**)

of ZIF-8 particles is seen in the composite structure and in addition, significant aggregation is not seen in the image [32].

pH influence on AMX and CFX removal

By examining the pH in the range of 2–8, removal of AMX and CFX with chitosan@polyacrylamide@ZIF-8 was determined and reported and the results are shown in Fig. 7. With increasing pH between 2 to 4, the percentage removal was enhanced and up to pH 4, it was decreased. Experiments illustrated the highest removal of AMX and CFX occurred at pH 4, it occurs because of, at this pH, adsorbates are ionized and take on negative charge [33]. Therefore, due to the positive charge of chitosan and polyacrylamide [amine groups (NH_2) of chitosan, polyacrylamide and ZIF-8 take on positive charge and released NH_3^+ and Zn^{2+} in the aqueous solution] and electrostatic interaction is established between the species and the adsorbent. Also, at pH < pk_a values, the drugs become protonated and due to the positive charge of the adsorbents, a repulsive force is created, so the adsorption is reduced ($pk_{a,CFX}$ = 3.45 and $pk_{a,AMX}$ = 4.18) [34, 35]. The experimental data show that in all of the pH values, the adsorbent contain ZIF-8 had more removal percentage than the CP. Asadi et al. investigated the pH of CFX removal from wastewater using UVC/sodium persulphate system in the range of 3–11 and optimum was reported pH = 3 [36].

Effect of adsorbent dosage

Amount of CP and CPZ as adsorbent for removal of AMX and CFX is shown in Fig. 8. The results indicated that with increasing the amount of CP and CPZ to 15 mg the removal percent is increased and then remained constant. With increasing the amount of adsorbent, the adsorbent surface and the active site for adsorption increases, so the removal percentage of AMX and CFX raised. Being constant or even decreasing the adsorption capacity of AMX and CFX with increasing the amount of CP and CPZ more than 15 mg is mainly because of the persistence of unsaturated sites during the process and also, overlap of active sites on the adsorbent. So 15 mg of CPZ and CP determined as an optimum amount and was utilized to continue the adsorption process. According to Fig. 8, CPZ had higher efficiencies than CP in all values [37, 38].

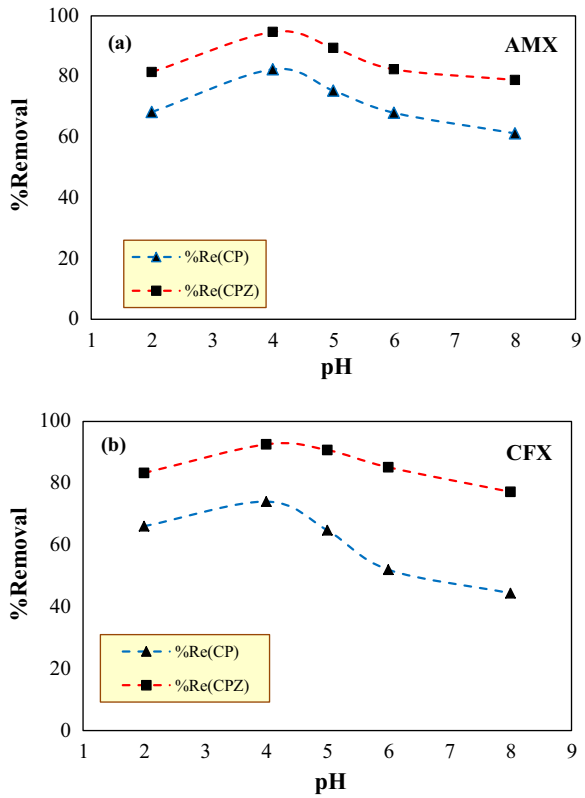

Fig. 7 pH influence on the percentage of AMX and CFX removal (initial concentration: 50 mg/L, amount of adsorbent: 15 mg, 40 min and 25 °C)

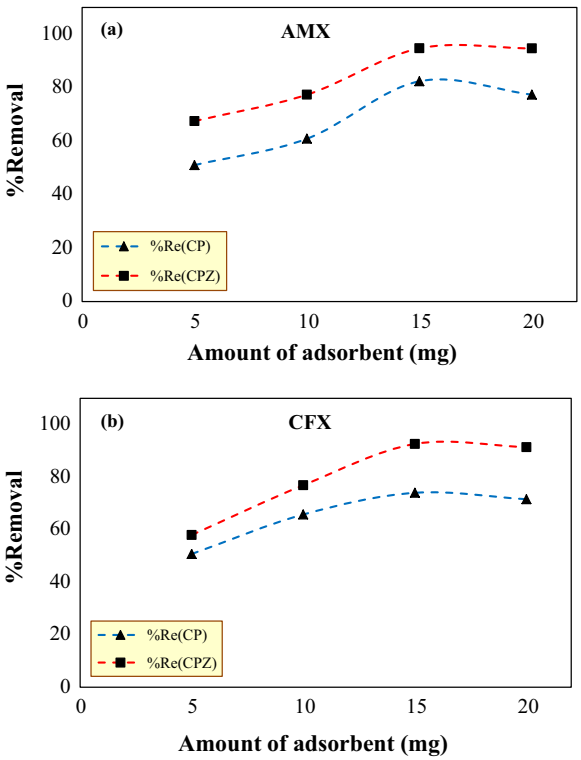

Fig. 8 Amount of adsorbent efficacy on the percentage of AMX and CFX removal (initial concentration: 50 mg/L, pH = 4, 40 min and 25 °C)

Adsorption experimental results in AMX removal used magnetic adsorbent by Jafari and et al. [39]. Research indicated that the removal efficiency reaches its maximum using 0.05 g/L of the adsorbent.

Effect of initial concentration

The influence of initial concentrations 25 to 200 mg/L on the adsorption rate was investigated. According to Fig. 9, with increasing the initial concentration, the removal percentage increased until 50 mg/L then it reached to the optimal adsorption point and decreased. At low concentrations, due to the low driving force the removal percentage was low, with increasing the initial concentration to 50 mg/L, the adsorbent is almost saturated with the drugs and with increasing the concentrations, active site was saturated by adsorbates, so it caused reduction in the removal rate. Overall, the results demonstrate that CPZ has higher removal of AMX and CFX than CP, indicating success in modifying CP adsorbent by adding ZIF-8 [40]. Initial concentration effect of CFX removal by GO–chitosan composite in batch media was investigated by Zeinep and et al. [41]; in the range of 20–100 mg/L and optimum was obtained 42 mg/L.

Effect of temperature

As shown in Fig. 10, with increasing temperature in all samples, decreasing in adsorption was achieved. In general, CPZ illustrated better adsorption for AMX and CFX than CP in all temperatures. The reduction in the rate of adsorption for CPZ was lower than CP, which proves the success of adsorbent modification and also improving in adsorption properties. In all tests, with increasing temperature the removal rate was reduced, so it can be found that AMX and CFX adsorption on CP and CPZ are exothermic [42]. Removal of AMX via hollow fiber was investigated by Pirom and et al. [43] and it was found that by increasing the temperature of the system from 278.15 to 318.15 K, extraction of AMX increased from 81.81 to 89.65%

Effect of contact time

The variation of contact time for adsorption of AMX and CFX simultaneously by CPZ is shown in Fig. 11. Over time up to 1 h, about 90% adsorption of CPZ adsorbent is take place for both AMX and CFX. As can be seen in the figures, at first 10 min the removal rate was increased rapidly and the adsorption process was

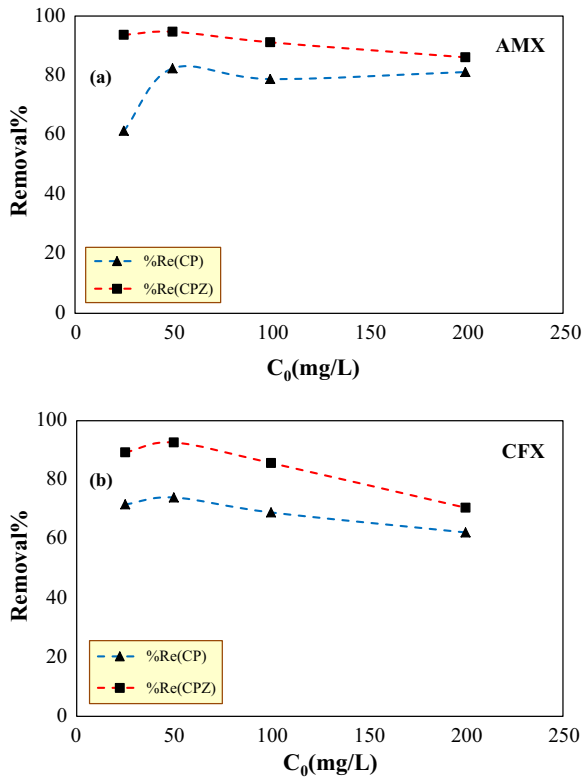

Fig. 9 Effect of initial concentration on AMX and CFX removal (amount of adsorbent: 15 mg, pH = 4, 30 min and 25 °C)

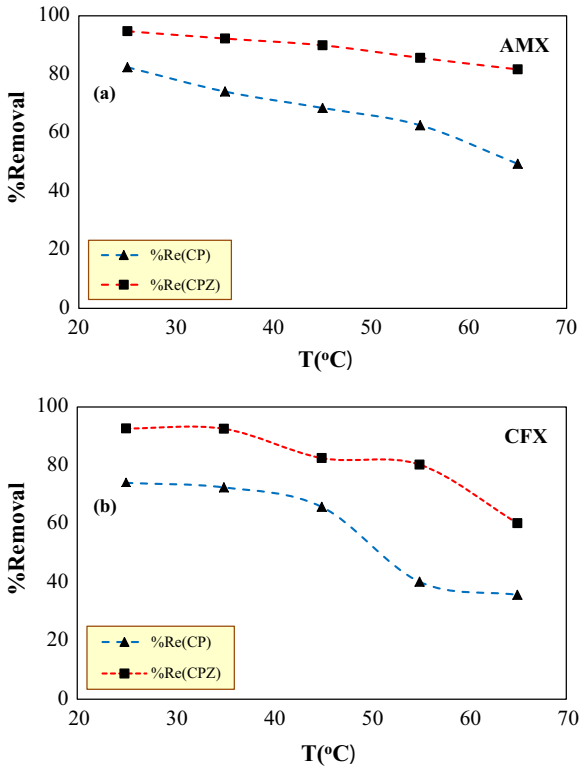

Fig. 10 Effect of temperature on the removal of AMX and CFX (amount of adsorbent = 15 mg, initial concentration: 50 mg/L in 5 mL of solutions, pH = 4, 30 min)

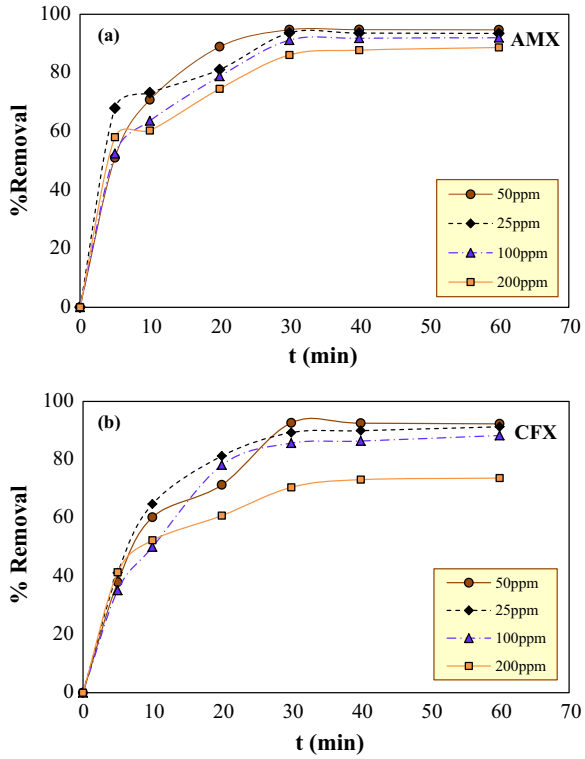

Fig. 11 Effect of contact time on AMX and CFX removal (initial concentration: 25 to 200 mg/L, amount of adsorbent: 15 mg in 5 mL of solutions, pH = 4, and T: 25 °C)

completed until 30 min, then equilibrium state was achieved.

Isotherm study

Experimental data for the adsorption of AMX and CFX on chitosan @ polyacrylamide@ZIF-8 were plotted by linear regressions, such as Langmuir, Freundlich, Temkin and Dubinin–Radushkevich models. Langmuir model is based on monolayer and homogeneous surface and the adsorption energy, remains constant during reaction. Langmuir model expressed by following equations:

$$q_e = \frac{q_m \cdot k_l \cdot C_e}{1 + k_l \cdot C_e}. \tag{3}$$

The above equation linearized by following [44]:

$$\frac{C_e}{q_e} = \frac{1}{k_l \cdot q_m} + \frac{1}{q_m} \cdot c_e, \tag{4}$$

where k_L (L/mg) is the Langmuir constant, q_m (mg/g) and q_e (mg/g) are maximum capacity and is equilibrium capacity of adsorption, respectively, C_e (mg/L) is the equilibrium AMX and CFX concentrations in residual.

The maximum adsorption capacity of AMX and CFX were calculated 910 and 588 mg/g, respectively (Table 1).

The Freundlich model expresses that the adsorption process occurs on heterogeneous surfaces. It can be found from the equation that the adsorption energy is decreased exponentially during the adsorption. The Freundlich model is expressed by the following equations:

Table 1 The values of parameters for isotherm models at 25 °C

Drugs	Isotherm models	Linear equations	Parameters	R^2
Amoxicillin	Langmuir	$\frac{C_e}{q_e} = \frac{1}{k_l \cdot q_m} + \frac{1}{q_m}.C_e$	$q_m = 910$ $k_l = 0.065$	0.97
	Freundlich	$\log q_e = \log k_f + (1/n)\log C_e$	$k_f = 68$ $n = 1.8$	0.95
	Temkin	$q_e = B \ln(A\, C_e)$	$A = 1.084$ $B = 169.21$	0.96
	Dubinin–Radushkevich	$\text{Ln}\ q_e = \ln q_m - k\varepsilon^2$	$q_m = 414$ $E = 0.707, k = 0.98$	0.90
Cefixime	Langmuir	$\frac{C_e}{q_e} = \frac{1}{k_l \cdot q_m} + \frac{1}{q_m}.C_e$	$q_m = 588$ $k_l = 0.07$	0.99
	Freundlich	$\log q_e = \log k_f + (1/n)\log C_e$	$k_f = 59.6$ $n = 1.98$	0.88
	Temkin	$q_e = B \ln(A\, C_e)$	$A = 1.26$ $B = 121.83$	0.98
	Dubinin–Radushkevich	$\text{Ln}\ q_e = \ln q_m - k\varepsilon^2$	$q_m = 385$ $E = 0.408, k = 0.34$	0.94

$$q_e = k_f \cdot C_e^{1/n}. \quad (5)$$

It can be linear by following [45]:

$$\log q_e = \log k_f + \left(\frac{1}{n}\right) \log C_e, \quad (6)$$

where K_f is the distribution coefficient and n is a correction factor and their values were predictable by $\mathrm{Ln}q_e$ vs. $\mathrm{Ln}C_e$ plot, are indicated in Table 1. As it is known, the value of n in this model was 2.28, which indicates that the desired adsorption has occurred.

Temkin isotherm assumes that the heat adsorption is linear and ignores very low and high concentrations and considers a homogeneous boundary energy distribution up to a portion of the maximal bonding energy.

Its expresses by equation below [46]:

$$q_e = B(\ln A) + B(\mathrm{lnCe}). \quad (7)$$

The correlation coefficient of the Temkin model is lower than other isotherms, which means experimental data do not justify the Temkin isotherm (Table 1).

The Dubinin–Radushkevich model expresses information about the adsorption type by the following equation:

$$\mathrm{Ln}q_e = \ln q_m - \beta\varepsilon^2, \quad (8)$$

where q_m(mg/g) is adsorption capacity, β and ε are D–R constant and Polanyi potential, respectively, that are dependent on the equilibrium concentration [47, 48]:

$$\varepsilon = \mathrm{RTln}(1 + 1/\mathrm{Ce}). \quad (9)$$

Results are presented in Table 1. The average free energy (E) in this model for AMX and CFX is calculated at 0.707 and 0.408 kJ/mol, respectively. If the calculated E is less than 8 kJ/mol, adsorption is physical. Therefore, physical adsorption is achieved in this work [49]. According to Table 1, the lines plotted for the Langmuir model had better conformity to experimental data of CFX and AMX, so the Langmuir model was superior.

As seen in Table 1, the lines plotted for the Langmuir model had better conformity to experimental data of CFX and AMX so the Langmuir mod was superior.

Maximum adsorption capacity of AMX and CFX on different adsorbents is listed in Table 2.

The results in Table 2 revealed chitosan@polyacrylamide@ZIF-8 has a more adsorption capacity than other adsorbents in the removal of AMX and CFX.

Adsorption kinetics

Being aware of the dynamic reaction and investigation of adsorption conditions are important in the kinetic process, several kinetic models for experimental data have been utilized to determine the adsorption mechanism and control step. To determine the kinetic type equation governing the adsorption process, intraparticle diffusion,

Table 2 Maximum adsorption capacity of various adsorbents used in the removal of CFX and AMX from aqueous solutions

Adsorbent	Adsorbate	q_{max} (mg/g)	Refs.
MIL-53(Al) metal–organic framework	Amoxicillin	758.5	[50]
Zinc oxide-coated carbon nanofiber	Amoxicillin	156	[51]
Carbon derived from protein-waste-doped	Amoxicillin, cefixime	25.2, 30.1	[52]
Pomegranate peel	Cefixime	181.81	[53]
Biosorbent prepared from pine cones	Cefixime	530	[54]
Chitosan@polyacrylamide@ZIF-8	Amoxicillin	910	Present study
Chitosan@polyacrylamide@ZIF-8	Cefixime	588	Present study

Table 3 Values of kinetic models parameters at different concentrations for AMX

C_0 (ppm)	Pseudo-first-order			Pseudo-second order				Intraparticle diffusion		
	K_{ad} (1/min)	$q_{e\cdot cal}$ (mg/g)	R^2	K_h (*10^4) (g/mg min)	$q_{e\cdot cal}$ (mg/g)	R^2	$q_{e\cdot exp}$ (mg/g)	K_p (mg/g $min^{0.5}$)	C (mg/g)	R^2
25	0.048	28	0.98	35	84	0.99	**78**	6.4	41.3	0.96
50	0.135	147	0.99	8.4	192	0.99	**157**	22.46	41.8	0.95
100	0.077	192	0.99	4.5	357	0.99	**303**	39.67	86.2	0.99
200	0.062	279	0.95	2.9	667	0.98	**574**	59.98	234.9	0.96

The data obtained from the experiment indicated in bold

Table 4 Values of kinetic models parameters at different concentrations for CFX

C_0 (ppm)	Pseudo-first-order			Pseudo-second order				Intraparticle diffusion		
	K_{ad} 1/min	$q_{e\cdot cal}$ mg/g	R^2	K_h(*10^4) g/mg min	$q_{e\cdot cal}$ mg/g	R^2	$q_{e\cdot exp}$ mg/g	K_p mg/g $min^{0.5}$	C mg/g	R^2
25	0.12	112	0.99	12.4	96	0.99	**74**	12	11.3	0.95
50	0.06	113	0.94	4.3	204	0.97	**154**	26.16	8.85	0.97
100	0.135	367	0.98	1.8	317	0.98	**285**	54.63	24.1	0.97
200	0.077	290	0.98	2.9	506	0.99	**469**	62.24	131.7	0.98

The data obtained from the experiment indicated in bold

pseudo-first-order and pseudo-second-order kinetic models were used. Weber and Morris provide the intraparticle diffusion velocity based on the function $t^{0.5}$ equation related to the Intraparticle diffusion model are expressed as follows [55]:

$$q_t = k_p \cdot t^{0.5} + C. \tag{10}$$

K_p and C are intraparticle diffusion velocity constant parameters that depend on the kinetics of the boundary layer. The calculated values with the correlation coefficient are presented in Tables 3 and 4 for AMX and CFX, respectively, demonstrated the intraparticle diffusion model is one of the steps determinative adsorption rates of CFX and AMX on CPZ.

The pseudo-first-order kinetic model is presented by the following equation [56]:

$$\mathrm{Ln}(q_e - q_t) = \ln(q_e) - k_1 \cdot t. \tag{11}$$

Linear plotting $\mathrm{Ln}(q_e - q_t)$ in terms of t, and the results are also collected in Tables 3 and 4, for AMX and CFX. The pseudo-first-order kinetic model indicates the rate of occupancy of the adsorbent active sites is proportional to the number of vacancies.

As can be seen in Tables 3 and 4, the large difference between the equilibrium adsorption capacity values (q_e) calculated from the pseudo-first order kinetic model (q_{cal}) and the experimental values (q_{exp}) for AMX and CFX indicates an inconformity between the results and experimental data were from pseudo-first-order kinetic model.

Pseudo-second-order model suggests the surface adsorption rate control phase from share or exchange of electrons between the adsorbent and the adsorbate. The linearized form of the pseudo-second-order equation is indicated by the equation below [57, 58]:

$$\frac{t}{q} = \frac{1}{k_h \cdot q_e^2} + \frac{t}{q_e}. \tag{12}$$

k_h is a constant of the pseudo-second-order (g/mg min). The adsorption of AMX and CFX on CPZ was plotted and the values of q_e and k_h were calculated by obtaining the slope and intercept of the lines drawn in different concentrations are given in Tables 3 and 4.

The low difference between the adsorption capacity of experimental data (q_{exp}) and calculated from the pseudo-second-order kinetic model (q_{cal}), for both AMX and CFX and also, higher correlation coefficient than others kinetic models, indicated the pseudo-second-order equation is an appropriate model for describing kinetics process of AMX and CFX on CPZ. Therefore, among all studied kinetic models in this work, the pseudo-second-order is predominant and the data have followed this model. Fakhri and et al. [59] investigated the adsorption characteristics of cephalosporins antibiotics and results showed the pseudo-second-order kinetic model with the activation energy of 7.6682 and 5.3745 kJ/mol for cephalexin and cefixime, respectively.

Conclusion

In the present study, the modified chitosan–polyacrylamide adsorbent was prepared by ZIF-8 for the simultaneous adsorption of AMX and CFX from aqueous solution. FTIR, XRD, TEM and SEM analysis revealed ZIF-8 was well placed in the structure of chitosan–polyacrylamide and the modified adsorbent had good porosity for adsorption. Various tests were performed to achieve the optimal parameters which: pH = 4, contact time 30 min, initial concentration 50 mg/L, temperature 25 °C and 15 mg of adsorbent are optimal values for both AMX and CFX adsorbents were determined. The linear isotherm models such as Langmuir, Freundlich, Temkin and Dubinin–Radushkevich were studied and the Langmuir isotherm prevailed in the comparison of data. Accordingly, maximum adsorption capacity for AMX and CFX with chitosan@polyacrylamide@ZIF-8 obtained 910 and 588 mg/g, respectively, which indicates the physicality adsorption process. Adsorption process kinetic was utilized to evaluate the reaction rate by kinetic models. The results illustrate that the experimental data had a better

agreement with the pseudo-second-order kinetic model. The investigation of different parameters in all experiments revealed, chitosan@polyacrylamide@ZIF-8 had more removal percent than chitosan@polyacrylamide. Therefore, chitosan@polyacrylamide composite modified by ZIF-8 can be chosen as a proper adsorbent for adsorption of drugs due to its high efficiency.

Author contributions
SBZ carried out the experiment. SBZ and AAA analyzed the data. SBZ and AAA wrote the manuscript. Both authors discussed the results and contributed to the final manuscript.

Funding
This work was supported by University of Mazandaran, Iran [1400/20235].

Availability of data and materials
All data generated or analyzed during this study are included in this published article.

Declarations

Ethics approval and consent to participate
The authors of this article have acted according to the ethical protocols and the information of the patients participating in this study will remain completely anonymous and all this information will remain protected after the study. Also, all the participants in this study have filled the consent form to participate in this study and all the purposes of the study have been fully explained to the participants. I consent to participate in the research project and the following has been explained to me: the research may not be of direct benefit to me. My participation is completely voluntary. My right to withdraw from the study at any time without any implications to me.

Consent for publication
I give my consent for the publication of identifiable details, which can include photographs, figures, table and details within the text to be published in this Journal.

Competing interests
The authors declare that they have no known competing financial interests or personal relationships that could have appeared to influence the work reported in this paper. The authors declare no competing interests.

Author details
[1]Department of Chemical Engineering, Technology and Engineering of Faculty, University of Mazandaran, Babolsar, Iran.

Received: 18 March 2023 Accepted: 28 July 2023
Published online: 03 August 2023

References

1. Liu X, Lee J, Ji K et al (2012) Potentials and mechanisms of genotoxicity of six pharmaceuticals frequently detected in freshwater environment. Toxicol Lett 211:70–76
2. Ghauch A, Tuqan A, Abou Assi H (2009) Antibiotic removal from water: elimination of amoxicillin and ampicillin by microscale and nanoscale iron particles. Environ Pollut 157:1626–1635
3. Balarak D, Mostafapour FK, Joghataei A (2016) Experimental and kinetic studies on penicillin G adsorption by Lemna minor. Br J Pharm Res 9:1–10
4. Ay F, Kargi F (2010) Advanced oxidation of amoxicillin by Fenton's reagent treatment. J Hazard Mater 179:622–627
5. Kümmerer K, Al-Ahmad A, Mersch-Sundermann V (2000) Biodegradability of some antibiotics, elimination of the genotoxicity and affection of wastewater bacteria in a simple test. Chemosphere 40:701–710
6. Fang Z, Chen J, Qiu X et al (2011) Effective removal of antibiotic metronidazole from water by nanoscale zero-valent iron particles. Desalination 268:60–67
7. de Franco MAE, de Carvalho CB, Bonetto MM et al (2017) Removal of amoxicillin from water by adsorption onto activated carbon in batch process and fixed bed column: kinetics, isotherms, experimental design and breakthrough curves modelling. J Clean Prod 161:947–956
8. Fallahzadeh RA, Mahvi AH, Meybodi MN et al (2019) Application of photo-electro oxidation process for amoxicillin removal from aqueous solution: modeling and toxicity evaluation. Korean J Chem Eng 36:713–721
9. Tabatabaei FS, Asadi-Ghalhari M, Aali R et al (2020) Removal of Cefixime from water using rice starch by response surface methodology. Avicenna J Med Biotechnol 12:230
10. Ghaithan AM, Mohammed A, Al-Hanbali A et al (2022) Multi-objective optimization of a photovoltaic-wind-grid connected system to power reverse osmosis desalination plant. Energy 251:123888
11. Haddaji C, Ennaciri K, Driouich A et al (2022) Optimization of the coagulation-flocculation process for vegetable oil refinery wastewater using a full factorial design. Process Saf Environ Prot 160:803–816
12. Choi J-H, Kim J-G, Kim H-B et al (2021) Dual radicals-enhanced wet chemical oxidation of non-biodegradable chemicals. J Hazard Mater 401:123746
13. González-Gaxiola O, Biswas A, Yildirim Y, Alshehri HM (2022) Highly dispersive optical solitons in birefringent fibers having Kerr law of refractive index by Laplace-Adomian decomposition. Optik 257:168788
14. Binaeian E, Babaee Zadvarzi S, Hoseinpour Kasgari A, Ebrahimnezhd Afrouzi M (2019) In situ synthesis of chitosan-grafted polyacrylamide loaded by TiO2 nanoparticles for the adsorption of sirius yellow K-CF from aqueous media: isotherm, kinetic and thermodynamic studies Ab va Fazilab. J Water Wastewater 30:16–30 (**in persian**)
15. Binaeian E, Mottaghizad M, Kasgary AH, Zadvarzi SB (2020) Bovine serum albumin adsorption by Bi-functionalized HMS, nitrilotriacetic acid-amine modified hexagonal mesoporous silicate. Solid State Sci 103:106194
16. Jia J, Du X, Zhang Q et al (2019) Z-scheme MgFe2O4/Bi2MoO6 heterojunction photocatalyst with enhanced visible light photocatalytic activity for malachite green removal. Appl Surf Sci 492:527–539
17. Pathania D, Katwal R, Sharma G et al (2016) Novel guar gum/Al2O3 nanocomposite as an effective photocatalyst for the degradation of malachite green dye. Int J Biol Macromol 87:366–374
18. Pham TD, Bui TT, Truong TTT et al (2020) Adsorption characteristics of beta-lactam cefixime onto nanosilica fabricated from rice HUSK with surface modification by polyelectrolyte. J Mol Liq 298:111981
19. Adriano WS, Veredas V, Santana CC, Gonçalves LRB (2005) Adsorption of amoxicillin on chitosan beads: Kinetics, equilibrium and validation of finite bath models. Biochem Eng J 27:132–137
20. Emami N, Farhadian M, Solaimany Nazar AR, Tangestaninejad S (2023) Adsorption of cefixime and lamotrigine on HKUST-1/ZIF-8 nanocomposite: isotherms, kinetics models and mechanism. Int J Environ Sci Technol 20:1645–1672
21. Bandforuzi SR, Hadjmohammadi MR (2019) Modified magnetic chitosan nanoparticles based on mixed hemimicelle of sodium dodecyl sulfate for enhanced removal and trace determination of three organophosphorus pesticides from natural waters. Anal Chim Acta 1078:90–100
22. Park KS, Ni Z, Côté AP et al (2006) Exceptional chemical and thermal stability of zeolitic imidazolate frameworks. Proc Natl Acad Sci 103:10186–10191
23. Leili M, Fazlzadeh M, Bhatnagar A (2018) Green synthesis of nano-zero-valent iron from Nettle and Thyme leaf extracts and their application for the removal of cephalexin antibiotic from aqueous solutions. Environ Technol 39:1158–1172
24. Li X, Liu Y, Zhang C et al (2018) Porous Fe2O3 microcubes derived from metal organic frameworks for efficient elimination of organic pollutants and heavy metal ions. Chem Eng J 336:241–252
25. Enayatpour B, Rajabi M, Yari M et al (2017) Adsorption/desorption study of proteins onto multi-walled carbon nanotubes and amino multi-walled carbon nanotubes surfaces as adsorbents. J Mol Liq 231:566–571
26. Kumar S, Koh J (2012) Physiochemical, optical and biological activity of chitosan-chromone derivative for biomedical applications. Int J Mol Sci 13:6102–6116

27. Nordin NAHM, Ismail AF, Misdan N, Nazri NAM (2017) Modified ZIF-8 mixed matrix membrane for CO2/CH4 separation. In: AIP Conference Proceedings. p 20091
28. Queiroz MF, Teodosio Melo KR, Sabry DA et al (2014) Does the use of chitosan contribute to oxalate kidney stone formation? Mar Drugs 13:141–158
29. Godwin Uranta K, Rezaei-Gomari S, Russell P, Hamad F (2018) Studying the effectiveness of polyacrylamide (PAM) application in hydrocarbon reservoirs at different operational conditions. Energies 11:2201
30. Nordin NAHM, Racha SM, Matsuura T et al (2015) Facile modification of ZIF-8 mixed matrix membrane for CO 2/CH 4 separation: synthesis and preparation. RSC Adv 5:43110–43120
31. Wang Y, Dai X, Zhan Y et al (2019) In situ growth of ZIF-8 nanoparticles on chitosan to form the hybrid nanocomposites for high-efficiency removal of Congo Red. Int J Biol Macromol 137:77–86
32. Binaeian E, Zadvarzi SB, Yuan D (2020) Anionic dye uptake via composite using chitosan–polyacrylamide hydrogel as matrix containing TiO2 nanoparticles; comprehensive adsorption studies. Int J Biol Macromol 162:150–162
33. Karimi S, Namazi H (2022) Magnetic alginate/glycodendrimer beads for efficient removal of tetracycline and amoxicillin from aqueous solutions. Int J Biol Macromol 205:128–140
34. Tiwari A, Singh A, Garg N, Randhawa JK (2017) Curcumin encapsulated zeolitic imidazolate frameworks as stimuli responsive drug delivery system and their interaction with biomimetic environment. Sci Rep 7:1–12
35. Hasanzadeh V, Rahmanian O, Heidari M (2020) Cefixime adsorption onto activated carbon prepared by dry thermochemical activation of date fruit residues. Microchem J 152:104261
36. Asadi-Ghalhari M, Mostafaloo R, Ghafouri N et al (2021) Removal of Cefixime from aqueous solutions via proxy electrocoagulation: modeling and optimization by response surface methodology. React Kinet Mech Catal 134:459–471
37. Harrache Z, Abbas M, Aksil T, Trari M (2019) Thermodynamic and kinetics studies on adsorption of Indigo Carmine from aqueous solution by activated carbon. Microchem J 144:180–189
38. Zadvarzi SB, Khavarpour M, Vahdat SM et al (2021) Synthesis of Fe3O4@ chitosan@ ZIF-8 towards removal of malachite green from aqueous solution: theoretical and experimental studies. Int J Biol Macromol 168:428–441
39. Jafari K, Heidari M, Rahmanian O (2018) Wastewater treatment for Amoxicillin removal using magnetic adsorbent synthesized by ultrasound process. Ultrason Sonochem 45:248–256
40. Tsai C-H, Chang W-C, Saikia D et al (2016) Functionalization of cubic mesoporous silica SBA-16 with carboxylic acid via one-pot synthesis route for effective removal of cationic dyes. J Hazard Mater 309:236–248
41. Ciğeroğlu Z, Küçükyıldız G, Erim B, Alp E (2021) Easy preparation of magnetic nanoparticles-rGO-chitosan composite beads: Optimization study on cefixime removal based on RSM and ANN by using Genetic Algorithm approach. J Mol Struct 1224:129182
42. Wu Y, Qi H, Li B et al (2017) Novel hydrophobic cotton fibers adsorbent for the removal of nitrobenzene in aqueous solution. Carbohydr Polym 155:294–302
43. Pirom T, Sunsandee N, Wongsawa T et al (2015) The effect of temperature on mass transfer and thermodynamic parameters in the removal of amoxicillin via hollow fiber supported liquid membrane. Chem Eng J 265:75–83
44. Binaeian E, Seghatoleslami N, Chaichi MJ (2016) Synthesis of oak gall tannin-immobilized hexagonal mesoporous silicate (OGT-HMS) as a new super adsorbent for the removal of anionic dye from aqueous solution. Desalin Water Treat 57:8420–8436
45. Dai X, Li X, Zhang M et al (2018) Zeolitic imidazole framework/graphene oxide hybrid functionalized poly (lactic acid) electrospun membranes: a promising environmentally friendly water treatment material. ACS Omega 3:6860–6866
46. Bayramoglu G, Yilmaz M (2018) Azo dye removal using free and immobilized fungal biomasses: isotherms, kinetics and thermodynamic studies. Fibers Polym 19:877–886
47. Smitha T, Santhi T, Prasad AL, Manonmani S (2017) Cucumis sativus used as adsorbent for the removal of dyes from aqueous solution. Arab J Chem 10:S244–S251
48. Kumar PS, Ramalingam S, Senthamarai C et al (2010) Adsorption of dye from aqueous solution by cashew nut shell: studies on equilibrium isotherm, kinetics and thermodynamics of interactions. Desalination 261:52–60
49. Zhong Q-Q, Yue Q-Y, Li Q et al (2011) Preparation, characterization of modified wheat residue and its utilization for the anionic dye removal. Desalination 267:193–200
50. Imanipoor J, Mohammadi M, Dinari M, Ehsani MR (2020) Adsorption and desorption of amoxicillin antibiotic from water matrices using an effective and recyclable MIL-53 (Al) metal–organic framework adsorbent. J Chem Eng Data 66:389–403
51. Chaba JM, Nomngongo PN (2019) Effective adsorptive removal of amoxicillin from aqueous solutions and wastewater samples using zinc oxide coated carbon nanofiber composite. Emerg Contam 5:143–149
52. Yu J, Kang Y, Yin W et al (2020) Removal of antibiotics from aqueous solutions by a carbon adsorbent derived from protein-waste-doped biomass. ACS Omega 5:19187–19193
53. Esmaeili Bidhendi M, Poursorkh Z, Sereshti H et al (2020) Nano-size biomass derived from pomegranate peel for enhanced removal of cefixime antibiotic from aqueous media: kinetic, equilibrium and thermodynamic study. Int J Environ Res Public Health 17:4223
54. Naghipoura D, Amoueib A, Ghasemid KT, Taghavie K (2020) Removal of cefixime from aqueous solutions by the biosorbent prepared from pine cones: kinetic and isotherm studies. Environment 11:14
55. Kulkarni MR, Revanth T, Acharya A, Bhat P (2017) Removal of crystal violet dye from aqueous solution using water hyacinth: equilibrium, kinetics and thermodynamics study. Resour Eff Technol 3:71–77
56. Revellame ED, Fortela DL, Sharp W et al (2020) Adsorption kinetic modeling using pseudo-first order and pseudo-second order rate laws: a review. Clean Eng Technol 1:100032
57. Yamini Y, Faraji M, Rajabi AA, Nourmohammadian F (2018) Ultra efficient removal of Basic Blue 41 from textile industry's wastewaters by sodium dodecyl sulphate coated magnetite nanoparticles: removal, kinetic and isotherm study. Anal Bioanal Chem Res 5:205–215
58. Oyelude EO, Awudza JAM, Twumasi SK (2017) Equilibrium, kinetic and thermodynamic study of removal of eosin yellow from aqueous solution using teak leaf litter powder. Sci Rep 7:1–10
59. Fakhri A, Adami S (2014) Adsorption and thermodynamic study of Cephalosporins antibiotics from aqueous solution onto MgO nanoparticles. J Taiwan Inst Chem Eng 45:1001–1006

Publisher's Note